Nuclear Engineering and Design 268 (2014) 104–112

Contents lists available at ScienceDirect

Nuclear Engineering and Design

journal homepage: www.elsevier.com/locate/nucengdes

Coupled analysis and improvements for Canadian-SCWR core design

Ammar Ahmad [a,b], Liangzhi Cao [a,b,*], Hongchun Wu [b]

[a] Key Laboratory of Thermo-Fluid Science and Engineering of MOE, School of Energy and Power Engineering, Xi'an Jiaotong University, Xi'an, Shaanxi 710049, China
[b] School of Nuclear Science and Technology, Xi'an Jiaotong University, Xi'an 710049, China

HIGHLIGHTS

- Coupled neutronics/thermal hydraulics analysis for recent Canadian-SCWR.
- Coolant density variation inside central flow tube of assembly was considered.
- An improved core design for Canadian-SCWR.
- Lower MCST and more flat radial power distribution.

ARTICLE INFO

Article history:
Received 7 September 2013
Received in revised form
16 December 2013
Accepted 24 December 2013

ABSTRACT

A coupled neutronics and thermal hydraulics analysis have been done for the recent Canadian SCWR, high efficiency re-entrant channel (HERC) design. The neutronics analysis was carried out by using a 3D fine mesh diffusion theory code and thermal hydraulics calculations were done by using single channel model. These two codes were coupled with each other by a link code. The axial variation of water density in the central flow tube has also been considered in the analysis. The maximum clad surface temperature for the original design was calculated to be very high, so some improvements in the channel design have also been proposed in this study. Moreover, a new core-loading scheme has been searched in order to get more flat radial power distribution and lower cladding surface temperature.

1. Introduction

Super critical water reactor (SCWR) is a nuclear power plant operating above thermodynamic critical point of water. The critical temperature and pressure for water are 374 °C and 22.1 MPa, respectively. SCWR is the only concept under the banner of generation IV nuclear reactor utilizing light water as coolant or moderator. SCWRs are considered as the next logical extension of existing water cooled reactors because of their simplification, as there is no phase change above critical point of water so unlike PWRs and BWRs, pressurizers, steam generators, recirculation pumps, steam separators and dryers are not required. Moreover it is more economical because of its high steam enthalpy which makes compact turbine system and higher thermal efficiency (Oka et al., 1992). Fossil fired power plants have been using super critical water as working fluid for more than 50 years. There are two main types of SCWRs:

- A large reactor pressure vessel containing the reactor core (fuelled) heat source, analogous to conventional PWRs and BWRs.
- Distributed pressure tubes or channels containing fuel bundles, analogous to conventional CANDU and RBMK nuclear reactors.

Russia and Canada have been focusing on the pressure-tube type SCWR (PT-SCWR) (Shan et al., 2010).

In R&D activities of past few years, many aspects of SCWR have been under considerations. Pre-conceptual core design for SCWR is one of them. Until now a large number of designs for SCWRs have been proposed. Both thermal (Yamaji et al., 2005) and fast (Yoo et al., 2006) neutron spectrum cores have been under consideration for SCWR pre-conceptual designs CANDU–SCWR is the pressure tube type SCWR proposed by Atomic Energy of Canada Limited (AECL) (Chow et al., 2007) having many advantages as compared to the pressure vessel type. The moderator and coolant are separated in this design so large density variation of SCW coolant has less effect on core neutronics (Yang et al., 2011). Some features of Canadian SCWRs are similar to that of the LWRs or BWRs (boiling water reactors) for example the arrangement of the core is vertical unlike conventional CANDU reactors, large axial variation of coolant density, long fuel assemblies instead of short fuel bundle columns, etc. The design presented in

* Corresponding author at: School of Nuclear Science and Technology, Xi'an Jiaotong University, 28 Xianning West Road, Xi'an 710049, China.
Tel.: +86 29 8266 3285; fax: +86 29 8266 7802.
E-mail addresses: caolz@mail.xjtu.edu.cn, caoliangzhi@gmail.com (L. Cao).

0029-5493/$ – see front matter © 2014 Elsevier B.V. All rights reserved.
http://dx.doi.org/10.1016/j.nucengdes.2013.12.045

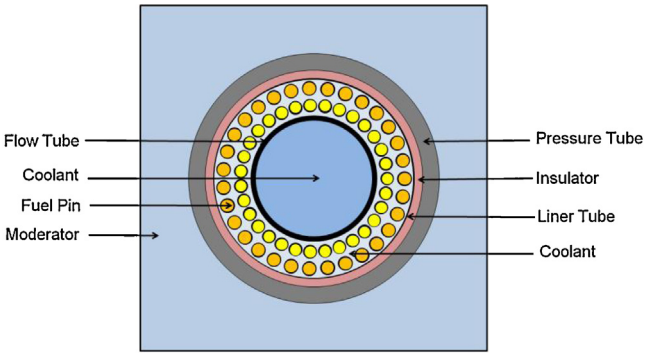

Fig. 1. Cross-sectional view of HERC design (Pencer et al., 2013).

Pencer et al. (2013) was chosen as the reference design for this analysis because it is the latest design for Canadian-SCWR and has some advantages over previous designs, e.g. better neutron moderation due to presence of coolant in central flow tube and two concentric fuel rings are providing balance in radial power distribution within the fuel assembly, etc. (Pencer et al., 2013).

Because of the large axial variation of the density, both neutronics and thermal hydraulics properties vary significantly over the entire length of fuel. The density of coolant can vary from a value of above 700 kg/m^3 to less than 100 kg/m^3. Conventional design studies using approach of constant coolant density throughout the active length of fuel cannot be applied here in the case of SCWRs. So the design studies of the SCWRs need coupled calculations for both neutronics and thermal hydraulics. The research done in the past has shown that the difference between the coupled and non-coupled calculations is noticeable (Waata, 2006).

In this study a 3D neutronics and thermal hydraulics calculations have been done on Canadian-SCWR high efficiency re-entrant channel (HERC) design (Pencer et al., 2013). Neutronics calculations were carried out by 3D fine mesh diffusion theory code where as thermal hydraulics calculations were based on single channel model. External coupling technique was used to couple these two codes; it means that there will be an exchange of data between these codes without modifying the source codes. Moreover in the analysis done by Pencer et al. (2013), the coolant density variation in the central flow tube was not investigated. In this study the SCW density variation inside the central flow tube has also been considered. Furthermore some improvements in channel design and core loading pattern have also been proposed in this research in order to decrease the maximum cladding surface temperature (MCST).

2. Materials and methods

2.1. Channel and core geometry

Cross-sectional view of 62 elements Canadian SCWR HERC design is shown in Fig. 1. The coolant first flows down from the central flow tube and then move upward through the space between the fuel pins carrying the heat of the fuel. Some of the geometric information is shown in Table 1. The details of the channel geometry and material can be seen in Pencer et al. (2013). The reactor core is a three batched fueled reactor core having 2540 MW of thermal power and 1200 MW of electric power. There are 336 fuel channels in the core. Each fuel channel contains a 500 cm long fuel assembly. The fuel assemblies are arranged in a 25 cm square lattice pitch. The total core height is 600 cm including 50 cm above and bottom heavy water reflectors (Pencer et al., 2013). Re-fuelling scheme is shown in Fig. 2.

Table 1
HERC geometry and dimensions (Dominguez et al., 2013).

Component	Dimensions
Central coolant	4.45 cm radius
Flow tube	4.45 cm inner radius, 0.1 cm thick
Inner pins (31)	0.415 cm radius, 5.30 cm circle radius
Outer pins (31)	0.465 cm radius, 6.55 cm circle radius
Cladding	0.06 cm thick
Liner tube	7.20 cm IR, 0.05 cm thick
Insulator	7.25 cm IR, 0.55 cm thick
Outer liner	7.80 cm IR, 0.05 cm thick
Pressure tube	7.85 cm IR, 1.2 cm thick
Fuel bundle heated length	500 cm

2.2. Calculation methodology

The burnup dependent macroscopic group constants for assembly were generated by a transport theory code DRAGON (Marleau et al., 2010) and were given as input to 3D fine mesh diffusion theory code CITATION (Fowler and Vondy, 1971) for core calculations. Microscopic cross-sections were taken from 69-group WIMSD library based on ENDFB-VII data. At the end of burnup calculations the energy groups were collapsed into 4 groups (2 thermal and 2 fast) and homogenized macroscopic cross-section were obtained as a function of burnup. All these macroscopic group constants were generated with all the expected water densities in the core. As CITATION has no function for burnup calculation so an auxiliary code was developed for core depletion calculations (Yang et al., 2011). The calculations were carried out using quarter core symmetry with corresponding 4 energy groups cross-sections obtained from assembly burnup calculations. The radial mesh size used was 1.6 cm × 1.6 cm and axial mesh size was 16.6 cm. As 3D core calculations with CITATION is very time taking so in order to save time a little larger axial mesh size was used. Thermal hydraulics calculations were based on a single channel model, in which each assembly was treated as one channel. The power profile for the whole core obtained from diffusion theory code was given as input to the thermal hydraulics code. The thermal calculations were carried out with two types of powers, maximum power and average power. Maximum power was used for flow rate search, satisfying the MCST criterion and using this flow rate distributions and average power for each assembly, the coolant density distribution was calculated (Zhao et al., 2013). This coolant density distribution was fed back as input to the neutronics code and the process was repeated until the convergence criteria for both the burnup and thermal calculations were met. Heat transfer coefficients were determined using Dittus Boelter correlation because it has high accuracy as compared to other correlations for single phase flows like SCW (Kamei et al., 2005).

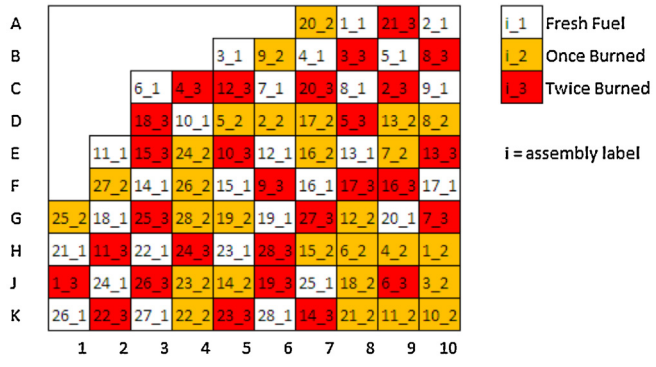

Fig. 2. Re-fuelling scheme for quarter core (Pencer et al., 2013).

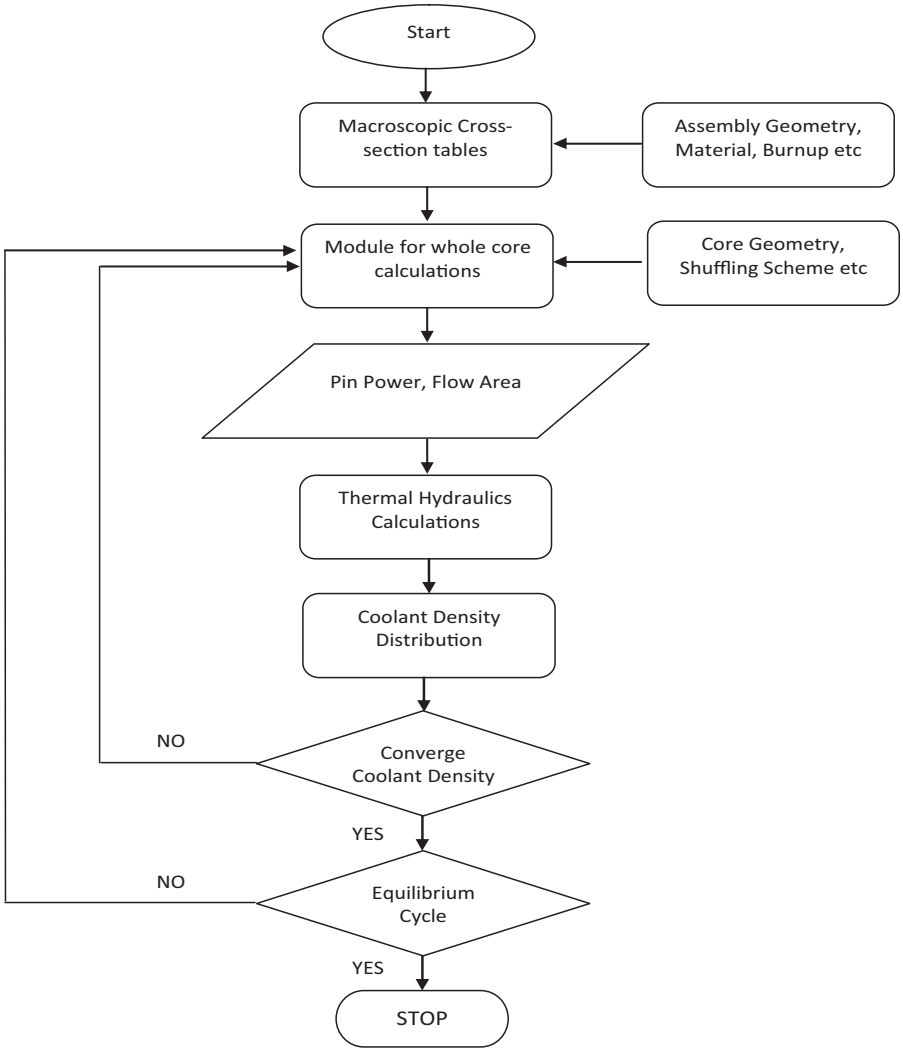

Fig. 3. Overall flow diagram of coupling scheme.

These two codes were coupled to each other by a link code. The input for one code was prepared from the output of the second code with the help of a link code. The overall flow diagram of the coupled system is shown in Fig. 3.

The equilibrium core was also searched during the procedure. The equilibrium core is defined as the core in which the burnup distribution and water density distribution at the beginning of (n)th cycle (BOC) are identical to those at the beginning of ($n+1$)th cycle. After determining all core design parameters, the first cycle is computed with neutronics/thermal hydraulics coupled system until water density distributions are converged. Then, according to fuel reload pattern, burnup distribution of the second cycle is obtained. The core calculations for one cycle of operation, followed by the shuffling of fuel assemblies, are repeated until the BOC burnup distribution is converged. Equilibrium cycle is achieved when BOC burnup distribution is converged (Zhao et al., 2013).

3. Results and discussion

The results for this research are divided into three parts. By using the calculation methodology described in previous section, firstly the analysis was done on reference core design model presented in Pencer et al. (2013). In this first step of analysis, the density of the coolant flowing through the central flow tube was considered as constant. In the second step of the analysis the density variation in the central flow tube was considered and in the third step some improvements in the assembly design and core loading pattern were proposed.

3.1. Results for reference design

The normalized radial power distribution for quarter core at beginning of cycle (BOC) and end of cycle (EOC) is shown in Fig. 4. The radial power peaking factor is 1.30 at BOC and 1.19 at EOC. This power profile is very much similar to the profile presented in (Pencer et al., 2013), with small relative difference of less than 10%. These differences are possibly due to the different calculation tools, cross-section library, number of groups and the effect of thermal hydraulics feedback. The analysis presented in Pencer et al. (2013) was based on lattice cell averaged two group cross-sections, while in this study the analysis is based on 4 group cross-sections.

Core average axial power distribution is shown in Fig. 5. The axial power peaking factors at BOC and EOC are 1.17 and 1.04, respectively. At BOC the power peaking factor is located at 300 cm from the bottom of the core and power profile is slightly asymmetric. The axial power distribution becomes flat and symmetric at EOC with power peaks located at 50 cm and 450 cm from the bottom of the core.

The coolant outlet temperature distribution at BOC and EOC for quarter core is shown in Fig. 6. The average coolant outlet

	1	2	3	4	5	6	7	8	9	10	
A							0.83	0.90	0.75	0.97	BOC
							0.94	1.01	0.85	1.06	EOC
B					0.97	0.89	0.97	0.79	0.99	0.80	
					1.08	0.99	1.05	0.86	1.07	0.87	
C			0.81	0.69	0.73	1.04	0.87	1.08	0.88	1.12	
			0.94	0.81	0.81	1.10	0.91	1.11	0.92	1.15	
D			0.69	0.92	0.93	1.03	1.03	0.93	0.99	1.00	
			0.81	1.01	1.00	1.05	1.03	0.93	1.00	1.01	
E		0.98	0.73	0.93	0.95	1.27	1.12	1.23	1.03	0.91	
		1.09	0.82	1.00	0.95	1.19	1.06	1.14	1.00	0.88	
F		0.90	1.04	1.04	1.27	1.06	1.30	0.98	0.94	1.21	
		1.00	1.10	1.06	1.19	0.97	1.16	0.90	0.87	1.11	
G	0.84	0.98	0.87	1.04	1.13	1.30	1.01	1.10	1.26	0.99	
	0.96	1.07	0.92	1.04	1.06	1.17	0.92	1.00	1.12	0.90	
H	0.92	0.80	1.09	0.94	1.23	0.98	1.09	1.15	1.13	1.12	
	1.03	0.88	1.13	0.94	1.15	0.90	1.00	1.04	1.02	1.01	
I	0.76	1.01	0.88	1.00	1.03	0.94	1.26	1.13	1.01	1.11	
	0.86	1.08	0.93	1.01	1.00	0.87	1.12	1.02	0.91	1.01	
J	0.99	0.82	1.14	1.01	0.91	1.21	0.99	1.11	1.11	1.14	
	1.08	0.89	1.16	1.02	0.88	1.11	0.90	1.01	1.00	1.02	

Fig. 4. Normalized radial power distribution at BOC and EOC.

temperature is 625 °C. At BOC coolant temperature ranges from 434 °C to 751 °C and it is higher towards the center of the core. At the end of cycle the outlet temperatures at the peripheral channels are higher than the temperatures of the central channels and ranges from 465 °C to 725 °C. The MCST distribution is shown in Fig. 7. The MCST at BOC is 930 °C and at EOC is 983 °C. MCST, both at BOC and EOC is very high exceeding the design limits.

3.2. Results by considering central water density variation

In the second part of the study, same analysis as described above was repeated by considering the axial density variation of water in central flow tube. Single channel thermal hydraulics code was modified to consider the heat transfer from coolant flowing through the spacing between the fuel to the central flow tube and then heat transferred from central flow tube to central water. The normalized radial power distribution for the core is shown in Fig. 8.

The radial power peaking factor is 1.29 at BOC and 1.19 at EOC. Core average axial power distribution is shown in Fig. 9. Axial power

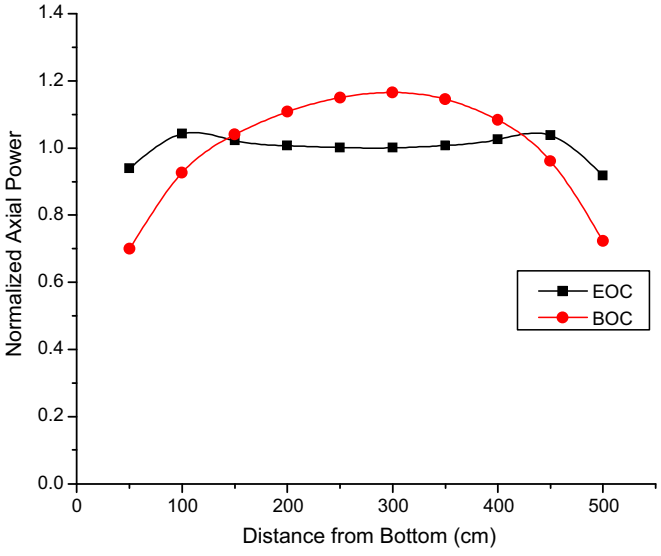

Fig. 5. Core normalized axial power distribution.

	1	2	3	4	5	6	7	8	9	10	
A							488	504	434	502	BOC
							546	557	465	544	EOC
B					492	491	650	521	651	642	
					539	538	711	569	703	702	
C			485	479	487	653	546	690	547	690	
			557	545	535	692	575	713	571	703	
D			516	606	623	666	677	643	689	681	
			600	674	668	678	676	640	695	688	
E		490	529	624	546	729	657	726	706	537	
		540	592	672	545	678	615	670	681	522	
F		552	657	604	730	746	751	719	567	746	
		621	700	617	680	678	663	654	526	672	
G	480	647	605	681	640	751	684	642	748	661	
	540	715	644	684	602	664	612	579	654	595	
H	573	526	696	558	726	719	701	738	733	716	
	650	580	725	558	673	656	631	657	652	640	
I	558	659	617	684	707	728	748	733	654	719	
	639	719	651	695	686	672	657	653	583	640	
J	572	526	699	687	562	747	643	727	713	721	
	634	573	718	699	548	678	581	651	636	638	

Fig. 6. Coolant outlet temperature distribution (1/4th core).

peaking factor at BOC and EOC are 1.16 and 1.04, respectively. Outlet coolant temperature and MCST distribution for quarter core are shown in Figs. 10 and 11. From Figs. 4, 5, 8 and 9, it can be seen that there is no obvious difference in radial and axial power distribution for both cases. This is due to the fact that the effect of water density variation on homogenized lattice cell average cross-section is very low. The maximum difference between the inlet and outlet temperature of central flow tube is only 15 °C, so this slight change in temperature will not affect the cell average cross-sections. But the effect on coolant outlet temperature distribution and MCST is noticeable as can be seen from Figs. 6, 7, 10 and 11. The average coolant outlet temperature is 625 °C. MCST at BOC and EOC for this case is 885 °C and 913 °C, respectively which is much lower than the previous case. This decrease in MCST is due to the fact

	1	2	3	4	5	6	7	8	9	10	
A							824	829	840	844	BOC
							959	962	958	957	EOC
B					830	801	839	843	847	828	
					955	946	951	938	936	927	
C			809	785	842	855	863	862	863	865	
			980	965	927	916	913	912	907	905	
D			821	840	852	866	868	863	862	843	
			958	935	902	888	887	888	888	904	
E		833	823	849	910	923	921	920	881	918	
		968	934	911	886	873	871	871	880	872	
F		807	860	898	925	908	926	901	926	926	
		963	926	890	876	869	871	864	863	863	
G	805	835	845	872	927	928	907	930	929	906	
	970	967	920	894	875	875	861	846	846	849	
H	838	856	869	901	924	903	906	906	906	904	
	981	951	925	893	876	868	847	844	843	844	
I	846	857	849	870	882	906	930	906	891	896	
	975	955	922	898	889	862	848	845	830	836	
J	854	865	874	852	913	928	904	898	891	890	
	983	946	923	919	885	869	849	843	826	823	

Fig. 7. MCST distribution (1/4th core).

	1	2	3	4	5	6	7	8	9	10	
A							0.84	0.91	0.76	0.98	BOC
							0.94	1.01	0.85	1.06	EOC
B					0.98	0.90	0.97	0.79	0.99	0.80	
					1.08	0.99	1.05	0.86	1.06	0.87	
C			0.82	0.70	0.73	1.04	0.87	1.08	0.88	1.12	
			0.95	0.81	0.81	1.09	0.91	1.11	0.92	1.14	
D			0.70	0.93	0.94	1.03	1.03	0.93	0.99	1.00	
			0.81	1.01	0.99	1.05	1.03	0.93	1.00	1.01	
E		1.00	0.74	0.94	0.95	1.26	1.12	1.22	1.02	0.91	
		1.09	0.81	0.99	0.95	1.19	1.06	1.14	1.00	0.89	
F		0.91	1.05	1.04	1.27	1.05	1.29	0.97	0.94	1.20	
		1.00	1.10	1.05	1.19	0.97	1.17	0.90	0.88	1.11	
G	0.86	0.99	0.88	1.04	1.13	1.29	1.01	1.09	1.24	0.98	
	0.97	1.06	0.92	1.04	1.06	1.17	0.92	1.00	1.12	0.90	
H	0.93	0.81	1.09	0.95	1.23	0.97	1.09	1.13	1.11	1.10	
	1.03	0.88	1.12	0.94	1.15	0.90	1.00	1.04	1.02	1.01	
I	0.77	1.02	0.89	1.00	1.03	0.93	1.24	1.11	1.00	1.10	
	0.86	1.08	0.92	1.01	1.00	0.87	1.12	1.02	0.91	1.01	
J	1.00	0.83	1.14	1.01	0.91	1.20	0.98	1.10	1.10	1.12	
	1.08	0.89	1.15	1.02	0.89	1.11	0.90	1.01	1.01	1.02	

Fig. 8. Normalized radial power distribution.

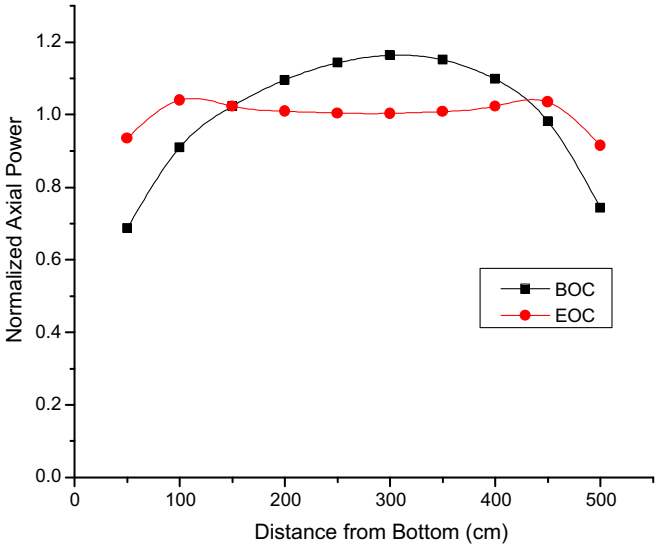

Fig. 9. Normalized axial power distribution.

	1	2	3	4	5	6	7	8	9	10	
A							487	504	434	501	BOC
							542	554	463	541	EOC
B					491	490	650	523	652	644	
					532	534	708	571	704	704	
C			484	478	489	653	549	690	550	691	
			548	538	533	689	577	713	575	707	
D			517	605	624	665	676	645	690	682	
			592	665	665	677	676	645	700	694	
E		487	529	623	546	725	656	723	708	539	
		527	584	664	544	677	618	673	689	527	
F		548	654	603	725	741	745	717	570	743	
		604	687	611	676	678	665	660	533	681	
G	477	640	603	678	638	744	682	644	745	659	
	525	692	633	675	600	663	616	587	663	602	
H	566	524	691	558	721	714	701	736	731	713	
	627	568	709	554	670	656	638	666	662	650	
I	555	654	615	681	703	726	745	730	656	719	
	621	699	640	686	682	675	663	661	595	653	
J	565	525	694	682	563	743	644	726	713	720	
	612	561	703	688	548	679	589	662	648	652	

Fig. 10. Coolant outlet temperature distribution.

	1	2	3	4	5	6	7	8	9	10	
A							785	790	800	803	BOC
							903	908	905	903	EOC
B					785	765	804	809	812	794	
					894	888	898	885	884	876	
C			768	750	805	818	826	825	827	828	
			914	901	869	861	861	861	859	857	
D			783	802	813	827	828	825	824	807	
			889	871	850	835	834	840	840	857	
E		785	785	809	866	879	877	877	844	874	
		894	866	849	831	821	822	823	836	825	
F		767	818	853	879	863	881	858	882	882	
		886	858	830	820	815	820	816	820	820	
G	761	788	803	831	881	882	865	885	885	863	
	891	889	853	832	820	820	814	804	804	804	
H	791	813	826	856	877	858	862	862	862	860	
	905	876	856	831	820	813	803	802	802	801	
I	803	814	807	826	837	861	884	862	849	858	
	894	878	853	836	830	812	803	802	793	798	
J	804	821	829	809	867	881	859	857	849	848	
	899	870	852	849	829	819	805	802	789	787	

Fig. 11. MCST distribution.

Table 2
Sensitivity analysis for central flow tube.

Flow tube inner radius (cm)	MCST BOC/EOC (°C)
3.55	924/985
4.45 (original design)	885/913
4.50	883/910
4.65	867/894
4.70	862/889

that by considering the heat transfer to the coolant in central flow tube, heat is now also transferred from the coolant surrounding the fuel to the coolant flowing in central flow tube. The coolant outlet temperature will be decreased by this effect and as a result MCST will also be decreased. The coolant outlet temperature can be maintained to desired level by adjusting coolant flow rate by specifying MCST criterion in thermal hydraulics code. MCST in this case is also much higher than the design limit 850 °C, so some modifications in design are required to decrease the MCST.

4. Improvements in channel and core design

4.1. Optimization of channel design

For channel design, several design options were investigated by varying the number of fuel pins, fuel pin dimensions, central flow tube thickness and central flow tube inner diameter, etc. The results for some of the design options are presented here. First of all, the sensitivity to the central flow tube diameter was examined. The diameter of the central flow tube was varied by keeping all the other parameters same and its effect on MCST was observed. The core loading pattern for this analysis was same as that of the previous analysis and is shown in Fig. 2. The results are shown in Table 2. The average outlet temperature for all the cases presented in Table 2 is 625 °C. The results show that by increasing the diameter of flow tube the MCST decreases because heat transfer coefficient between coolant and cladding increases. This will be discussed in detail in Section 4.3. So, for the new design 4.65 cm inner radius for flow tube was selected. It can be seen from Table 2 that the MCST for 4.70 cm is less than that of 4.65 cm but if 4.70 cm is selected as the radius for flow tube then the clearance between fuel pins and central flow tube will become very less, i.e. 0.25 mm which will be a challenge from manufacturing perspective. There is a decrease of

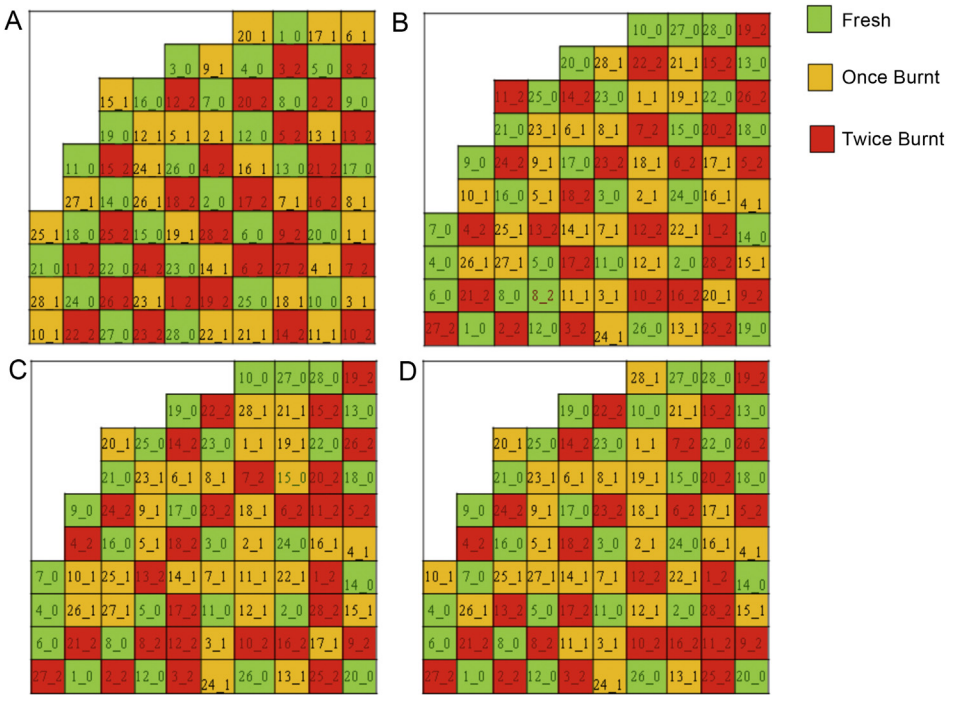

Fig. 12. Core loading patterns.

18 °C in MCST when central flow tube inner radius was increased from 4.45 cm to 4.65 cm.

Now in the next step the flow tube radius was selected as 4.65 cm and number of fuel pins per ring was varied to observe the sensitivity of MCST to number of fuel pins. The results are shown in Table 3. The results show that when number of pins per ring is decreased from 31 to 30, MCST increases while when number of pins is increased to 32 or 33 the MCST decreases. On the basis of these results the 32 number of pins per ring were selected. It can be seen from Table 3 that the MCST for 33 pins per ring is less than that of 32 pins case but if 33 fuel pins are selected then physical spacing between the fuel pins in a ring will become very small, i.e. 0.5 mm. In this study fuel rod gap was set to be around 1 mm by referring to the core designs presented in (Uchikawa et al., 2007)

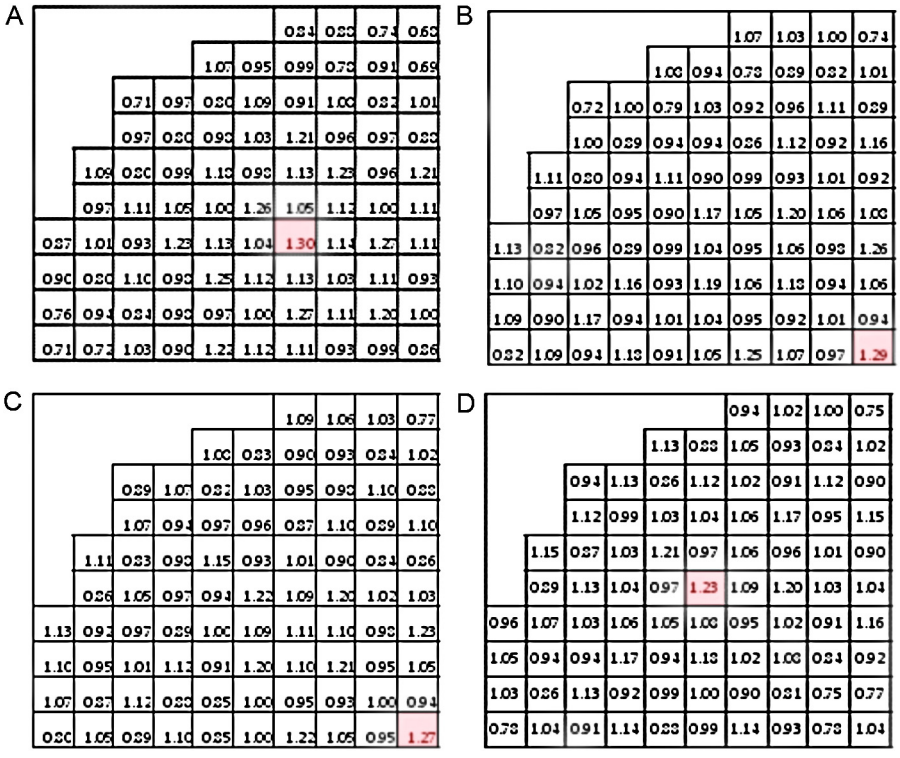

Fig. 13. Power distribution (BOC) for core loading patterns.

Table 3
Sensitivity analysis for number of fuel pins.

Number of fuel pins per ring	MCST BOC/EOC (°C)
30	878/914
31	867/894
32	860/880
33	847/868

Table 4
Proposed design geometry and dimensions.

Component	Dimensions
Central coolant	4.65 cm radius
Flow tube	4.65 cm inner radius, 0.1 cm thick
Inner pins (32)	0.415 cm radius, 5.30 cm circle radius
Outer pins (32)	0.465 cm radius, 6.55 cm circle radius
Cladding	0.06 cm thick
Liner tube	7.20 cm IR, 0.05 cm thick
Insulator	7.25 cm IR, 0.55 cm thick
Outer liner	7.80 cm IR, 0.05 cm thick
Pressure tube	7.85 cm IR, 1.2 cm thick
Fuel bundle heated length	500 cm

and (Cao et al., 2008). So either fuel pin radius has to be decreased or fuel ring radius has to be increased to consider 33 fuel pins per ring. This change in fuel pin radius or fuel ring radius will also affect the MCST; this affect was not studied in the present research. So in order to avoid major modifications in the channel design, 32 fuel pins per ring were selected for new proposed design.

4.2. Core loading pattern

Core loading pattern has strong influence on the performance of the core. MCST can also be decreased by selecting the core loading pattern having more flat power distribution. Several core loading patterns were investigated in order to achieve more flat radial power profile and low power peaking factor which in turn will decrease the cladding surface temperature. Some of them are shown in Fig. 12. The power distributions at BOC for these loading patterns are shown in Fig. 13. Core loading pattern having lowest power peaking factor was searched. For pattern A, the peak is located in fresh fuel, so in pattern B the fresh fuel were distributed in the core in such a way, that the less number of fresh fuel were in the center of the core and there were twice burnt fuel assemblies in the vicinity of each fresh fuel assembly. In Pattern B and C the peaks are located in the center of the core so in pattern D more twice burnt fuel assemblies were added near the center of the core in order to compensate the peak power. In this way by optimizing several patterns, pattern D was searched having lowest peak of 1.23 as shown in Fig. 13. So it is selected as the loading pattern for this design.

4.3. Results for proposed design

The final design parameters for fuel channel are shown in Table 4. The central flow tube internal radius is increased from 4.45 cm to 4.65 cm and number fuel pins in each ring is increased from 31 to 32. The fuel loading pattern and shuffling scheme for the design is shown in Fig. 14. Fig. 15 shows the normalized radial power distribution for proposed core design. The radial power peaking factors at BOC and EOC are 1.23 and 1.15, respectively, which is much lower than the previous design. Core average axial power distribution is shown in Fig. 16. Axial power peaking factors at BOC and EOC are 1.17 and 1.04, respectively. Outlet temperature and MCST distribution are shown in Figs. 17 and 18. The coolant average outlet temperature is 625 °C. MCST at BOC and EOC are 844 °C and 854 °C which are near the design criteria. As compared

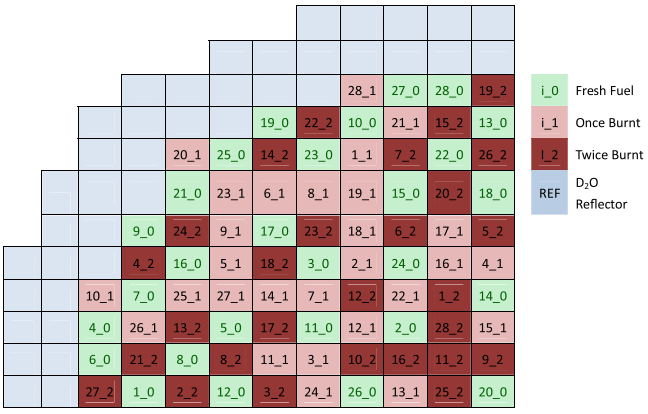

Fig. 14. Proposed core loading pattern for quarter core.

	1	2	3	4	5	6	7	8	9	10	
A							0.94	1.02	1.00	0.75	BOC
							0.97	1.05	1.04	0.81	EOC
B					1.13	0.88	1.05	0.93	0.84	1.02	
					1.10	0.88	1.05	0.96	0.87	1.05	
C			0.94	1.13	0.86	1.12	1.02	0.91	1.12	0.90	
			0.94	1.09	0.86	1.09	1.02	0.92	1.11	0.91	
D			1.12	0.99	1.03	1.04	1.06	1.17	0.95	1.15	
			1.09	0.98	1.02	1.02	1.04	1.14	0.94	1.13	
E		1.15	0.87	1.03	1.21	0.97	1.06	0.96	1.01	0.90	
		1.11	0.86	1.01	1.14	0.94	1.03	0.94	1.00	0.90	
F		0.89	1.13	1.04	0.97	1.23	1.09	1.20	1.03	1.04	
		0.89	1.10	1.02	0.93	1.15	1.05	1.14	1.02	1.04	
G	0.96	1.07	1.03	1.06	1.05	1.08	0.95	1.02	0.91	1.16	
	0.99	1.06	1.02	1.04	1.02	1.05	0.93	1.02	0.92	1.15	
H	1.05	0.94	0.94	1.17	0.94	1.18	1.02	1.08	0.84	0.92	
	1.07	0.97	0.94	1.14	0.92	1.14	1.02	1.09	0.88	0.97	
I	1.03	0.86	1.13	0.92	0.99	1.00	0.90	0.81	0.75	0.77	
	1.06	0.89	1.12	0.92	0.99	1.00	0.91	0.85	0.82	0.84	
J	0.78	1.04	0.91	1.14	0.88	0.99	1.14	0.93	0.78	1.04	
	0.83	1.06	0.92	1.12	0.89	1.01	1.14	0.98	0.86	1.11	

Fig. 15. Normalized radial power distribution for proposed design.

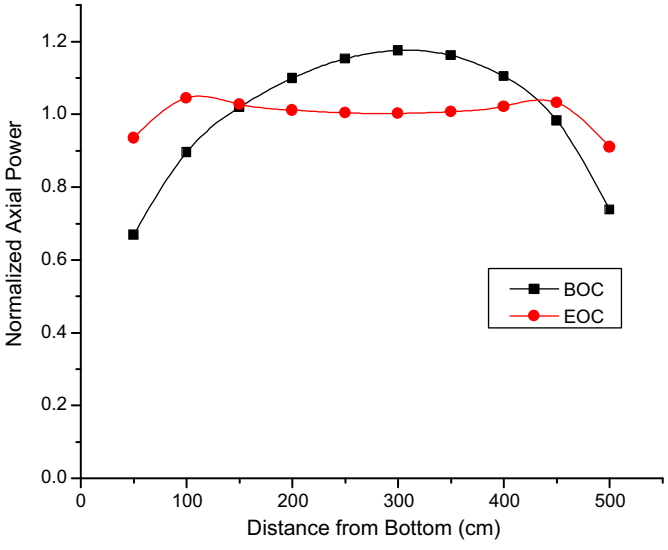

Fig. 16. Core averaged axial power distribution.

Table 5
Summary of results.

Parameters	Results presented in Pencer et al. (2013)	This study		
		Reference design	Central water density variation	New proposed design
Operating pressure (MPa)	25	25	25	25
Thermal/electrical power (MW)	2540/1200	2540/1200	2540/1200	2540/1200
Average initial wt% of PuO_2	13%	13%	13%	13%
Average exit burnup (MWd/kg)	58.6	58.6	58.6	56.8
Excess reactivity BOC/EOC (mk)	108.9/10.0	146.9/54.8	146.5/54.2	150.4/62.26
Cycle length EFPD	425	425	425	425
Channel power peaking factor (BOC/EOC)	1.31/1.22	1.30/1.19	1.29/1.19	1.23/1.15
Axial power peaking factor	1.18/1.05	1.17/1.04	1.16/1.04	1.17/1.04
Average outlet temperature (°C)	–	625	625	625
MCST (BOC/EOC) (°C)	–	930/983	885/913	844/854

	1	2	3	4	5	6	7	8	9	10	
A							508	526	516	431	BOC
							525	539	535	448	EOC
B					518	518	686	670	550	680	
					505	521	691	699	573	702	
C			474	524	546	689	689	565	706	681	
			472	509	541	672	691	568	701	691	
D			595	668	692	707	640	720	587	711	
			576	661	680	692	627	693	581	692	
E		511	603	624	726	710	704	650	688	654	
		497	598	613	685	681	682	632	682	650	
F		578	693	707	572	732	645	719	689	616	
		579	673	693	550	684	620	683	682	614	
G	503	688	690	709	693	707	627	681	551	688	
	515	687	689	697	674	683	609	677	554	678	
H	599	677	570	719	562	712	626	671	588	571	
	608	699	571	696	551	685	626	674	618	602	
I	589	558	709	639	680	683	668	643	641	623	
	605	577	703	637	684	688	683	682	703	685	
J	566	685	567	722	621	664	684	624	517	641	
	603	701	573	710	627	675	684	668	562	685	

Fig. 17. Coolant outlet temperature distribution.

to original design, MCSTs for both BOC and EOC are decreased by 40 °C and 60 °C, respectively.

As in proposed design the radius for central flow tube and number of fuel rods have been increased, both of these factors made the coolant area around the fuel to decrease. In other words it can be said that hydraulic diameter was decreased. When the coolant area or hydraulic diameter was decreased, coolant mass flux was increased which made the heat transfer coefficient between cladding and coolant to increase so as a result cladding surface temperature was decreased. The results for above study are summarized in Table 5. Average exit burnup for proposed design is less and excess reactivity is more than that presented in Pencer et al. (2013) as shown in Table 5. So either cycle length for the proposed design can be increased or initial enrichment can be decreased. Significant decrease in channel peaking factor and cladding surface temperature for proposed design can also be observed from Table 5.

	1	2	3	4	5	6	7	8	9	10	
A							813	813	812	813	BOC
							847	854	854	849	EOC
B					842	802	811	789	813	813	
					822	825	829	833	846	846	
C			838	838	821	818	798	821	821	799	
			820	821	814	811	810	822	823	812	
D			836	803	803	804	822	822	823	822	
			822	806	803	802	802	803	820	805	
E		844	802	826	830	809	806	795	794	801	
		821	812	802	798	791	792	800	800	792	
F		820	818	804	830	827	821	820	789	818	
		824	811	803	796	790	792	792	801	794	
G	798	819	799	799	804	804	795	795	806	806	
	834	836	809	805	793	790	795	795	802	802	
H	818	792	819	819	818	817	803	802	769	800	
	851	830	813	807	797	795	803	803	814	804	
I	817	817	820	794	788	786	781	768	754	764	
	852	839	823	813	805	801	800	810	823	813	
J	810	815	821	818	780	776	795	762	769	775	
	854	844	828	822	808	807	808	817	838	836	

Fig. 18. MCST distribution.

5. Conclusion

A coupled neutronics and thermal hydraulics analysis was done for CANDU–SCWR HERC design. The axial density variation in central flow tube of the channel was considered and its substantial effect on core thermal hydraulics was observed. The MCST for original design was found to be very high. An improved assembly design and loading pattern were also proposed in order to decrease the cladding surface temperature. The radial power profile for proposed design is more flat having low power peaking factor and there is a significant reduction in MCST from 983 °C to 854 °C. The excess reactivity at EOC for proposed design was found to be higher than the previous design, which means that either core cycle length can be increased or initial fuel enrichment can be decreased. The proposed design still needs some improvements and it should be further optimized on the basis of sub-channel analysis to minimize the MCST which is slightly higher than 850 °C. Moreover the study for control rods should also be considered in future.

Acknowledgement

This work was financially supported by the National Science Foundation of China (approved number 91126005 and 91226106).

References

Cao, L., Oka, Y., Ishiwatari, Y., et al., 2008. Fuel, core design and subchannel analysis of a superfast reactor. Journal of Nuclear Science and Technology 45, 138–148.

Chow, C.K., Khartabil, H.F., 2007. Conceptual fuel channel designs for CANDU–SCWR. Special issue on the 3rd international symposium on SCWR. Nuclear Engineering and Technology 40 (2), 139–146.

Dominguez, A.N., Onder, E.N., Pencer, J., et al., 2013. Canadian SCWR bundle optimization for the new fuel channel design. In: The 6th International Symposium on Supercritical Water-Cooled Reactors, ISSCWR-6, Shenzhen, Guangdong, China.

Fowler, T.B., Vondy, D.R., 1971. Nuclear Reactor Core Analysis Code CITATION, ORNLTM-2496. Oak Ridge National Laboratory, Oak ridge, USA.

Kamei, K., Yamaji, A., Ishiwatari, Y., et al., 2005. Fuel and core design of super light water reactor with low leakage fuel loading pattern. Journal of Nuclear Science and Technology 43 (2), 129–139.

Marleau, G., Hébert, A., Roy, R., 2010. A User's Guide for DRAGON Version 4. Institut de génie nucléaire, Département de génie mécanique, École Polytechnique de Montsréal, Montreal, Canada.

Oka, Y., Koshizuka, S., Yamasaki, T., 1992. Direct cycle light water reactor operating at supercritical pressure. Journal of Nuclear Science and Technology 29 (6), 585–588.

Pencer, J., Watts, D., Colton, A., et al., 2013. Core Neutronics for the Canadian SCWR conceptual design. In: The 6th International Symposium on Supercritical Water-cooled Reactors ISSCWR-6, Shenzhen, Guangdong, China.

Shan, J., Chen, W., Rhee, B.W., et al., 2010. Coupled neutronics/thermal-hydraulics analysis of CANDU–SCWR fuel channel. Annals of Nuclear Energy 37, 58–65.

Uchikawa, S., Okubo, T., Kugo, T., et al., 2007. Conceptual design of innovative water reactor for flexible fuel cycle (FLWR) and its recycle characteristics. Journal of Nuclear Science and Technology 44 (3), 277–284.

Waata, C., 2006. Coupled Neutronics/Thermal-Hydraulics Analysis of a High Performence Light-Water Reactor Fuel Assembly. Institute of Nuclear Technology and Energy System, University of Stuttgart, Stuttgart, Germany.

Yamaji, A., Kaemi, K., Oka, Y., et al., 2005. Improved core design of high temperature supercritical-pressure light water reactor. Annals of Nuclear Energy 32 (7), 651.

Yang, P., Cao, L., Wu, H., et al., 2011. Core design study on CANDU–SCWR with 3D neutronics/thermal hydraulics coupling. Nuclear Engineering and Design 241, 4714–4719.

Yoo, J., Ishiwatari, Y., Oka, Y., et al., 2006. Conceptual design of compact supercritical water-cooled fast reactor with thermal hydraulic coupling. Annals of Nuclear Energy 33, 945–956.

Zhao, C., Cao, L., Wu, H., et al., 2013. Conceptual design of a supercritical water reactor with double-row-rod assembly. Progress in Nuclear Energy 63, 86–95.